

Original Article

Conditional Deletion of *Sost* in MSC-derived lineages Identifies Specific Cell Type Contributions to Bone Mass and B Cell Development[†]

Cristal S. Yee^{1,2#}, Jennifer O. Manilay^{2#}, Jiun C. Chang^{1,2}, Nicholas R. Hum¹, Deepa K. Muruges¹, Jamila Bajwa², Melanie E. Mendez^{1,2}, Aris E. Economides³, Daniel J. Horan⁴, Alexander G. Robling⁴ and Gabriela G. Loots^{1,2*}

¹*Lawrence Livermore National Laboratories, Physical and Life Sciences Directorate, Livermore, CA 94550, USA.*

²*University of California-Merced, Molecular Cell Biology Unit, School of Natural Sciences, Merced, CA, USA*

³*Regeneron, Tarrytown, NY, USA*

⁴*Indiana University School of Medicine, Department of Anatomy & Cell Biology, Indianapolis, IN 46202, USA.*

¹Biology and Biotechnology Division,
Lawrence Livermore National Laboratory
7000 East Avenue, L-452
Livermore, CA 94550

*Author for correspondence (e-mail: loots1@llnl.gov)

#Drs. Yee and Manilay contributed equally to this work

Additional Supporting Information may be found in the online version of this article.

Initial Date Submitted October 10, 2017; Date Revision Submitted April 26, 2018; Date Final Disposition Set April 28, 2018

This is the author's manuscript of the article published in final edited form as:

Yee, C. S., Manilay, J. O., Chang, J. C., Hum, N. R., Muruges, D. K., Bajwa, J., ... Loots, G. G. (2018). Conditional Deletion of *Sost* in MSC-derived lineages Identifies Specific Cell Type Contributions to Bone Mass and B Cell Development. *Journal of Bone and Mineral Research*, 0(ja). <https://doi.org/10.1002/jbmr.3467>

ABSTRACT

Sclerostin (Sost) is a negative regulator of bone formation and blocking its function *via* antibodies has shown great therapeutic promise by increasing both bone mass in humans and animal models. Sclerostin deletion in *Sost* knockout mice (*Sost*^{-/-}) causes high bone mass (HBM) similar to Sclerosteosis patients. *Sost*^{-/-} mice have been shown to display an up to 300% increase in bone volume/total volume (BV/TV), relative to aged matched controls, and it has been postulated that the main source of skeletal Sclerostin is the osteocyte. To understand the cell-type specific contributions to the HBM phenotype described in *Sost*^{-/-} mice, as well as to address the endocrine and paracrine mode of action of sclerostin, we examined the skeletal phenotypes of conditional *Sost* loss-of-function (*Sost*^{iCOIN/iCOIN}) mice with specific deletions in (1) the limb mesenchyme (*Prx1-Cre*; targets osteoprogenitors and their progeny); (2) mid-stage osteoblasts and their progenitors (*Col1-Cre*); (3) mature osteocytes (*Dmp1-Cre*) and (4) hypertrophic chondrocytes and their progenitors (*ColX-Cre*). All conditional alleles resulted in significant increases in bone mass in trabecular bone in both the femur and lumbar vertebrae, but only *Prx1-Cre* deletion fully recapitulated the amplitude of the HBM phenotype in the appendicular skeleton and the B cell defect described in the global knockout. Despite wildtype expression of Sost in the axial skeleton of *Prx1-Cre* deleted mice, these mice also had a significant increase in bone mass in the vertebrae, but the Sclerostin released in circulation by the axial skeleton did not affect bone parameters in the appendicular skeleton. Also, both *Col1* and *Dmp1* deletion resulted in a similar 80% significant increase in trabecular bone mass, but only *Col1* and *Prx1* deletion resulted in a significant increase in cortical thickness. We conclude that several cell types within the *Prx1*-osteoprogenitor derived lineages contribute significant amounts of Sclerostin protein to the paracrine pool of Sost, in bone. This article is protected by copyright. All rights reserved

Introduction

Sclerostin (*Sost*) is a secreted Wnt antagonist that primarily functions to negatively regulate bone formation by preventing the propagation of Wnt signaling through the low-density lipoprotein receptor-related proteins (LRP4/5/6 Wnt co-receptors) in osteoblasts, pre-osteocytes, and osteocytes.^(1,2) Patients carrying homozygous *SOST* null mutations (Sclerosteosis) display generalized high bone mass (HBM),^(3,4) a phenotype that is recapitulated in *Sost* knockout mice (*Sost*^{-/-}).^(5,6) Conversely, overexpression of *SOST* in transgenic mice (*SOST*^{tg}) results in osteopenia.⁽⁷⁾ Shortly after the gene responsible for Sclerosteosis was cloned, *SOST* transcripts were reported in bone, bone marrow, cartilage, kidney, liver, lung, heart and pancreas^(3,4), however, histological examination determined that the osteocytes within cortical and trabecular bone were a dominant source of sclerostin.^(8,9) These observations support the hypothesis that the HBM phenotype in both patients and mice is due to sclerostin deficiency in osteocytes, and that sclerostin acts in a paracrine manner.⁽¹⁰⁾

More recent reports have provided new evidence that sclerostin may also act in an endocrine manner. Sclerostin serum levels were found to correlate with bone phenotypes, and several groups have shown that serum sclerostin levels are elevated in post-menopausal compared to pre-menopausal women.⁽¹¹⁻¹³⁾ Estrogen treatment administered to post-menopausal women significantly decreased serum sclerostin and mRNA levels in bone biopsies compared to untreated post-menopausal women⁽¹³⁻¹⁵⁾, suggesting that estrogen may function to inhibit *Sost* expression/production.^(13,16) Similarly, an increase in *SOST* serum levels were documented for aging men and women.⁽¹³⁾

Sclerostin serum levels are affected by age, gender, hormone and disease status, suggesting that sclerostin serum levels could impact bone physiology. Osteocytes are the likely source of most of the circulating sclerostin found in serum. Thus, all of the above mentioned sclerostin-modulating factors could control sclerostin transcriptionally or post-transcriptionally, in bone. Another unresolved issue is whether bone-associated cell types other than osteocytes also contribute to the sclerostin protein pool locally and systemically, including osteoblasts, osteoclasts, bone lining cells, mesenchymal stem cells or other progenitors along the osteoblastic- and chondrogenic- lineages. To understand the cell-type specific contributions to the HBM phenotype described in *Sost*^{-/-} mice, as well as to address the endocrine and paracrine mode of action of sclerostin, we examined the skeletal phenotypes of conditional *Sost* loss-of-function (*Sost*^{iCOIN/iCOIN}) mice with specific deletions in (1) the limb mesenchyme (*Prx1-Cre*-driven recombination) which targets osteoprogenitors and their progeny; (2) mid-stage osteoblasts and their progenitors (*Col2.3-Cre*-driven recombination); (3) early-stage osteocytes (*Dmp1-Cre*-driven recombination) and (4) hypertrophic chondrocytes and their progenitors (*ColX-Cre*).

We were particularly interested in determining whether any of these mice phenocopy the global *Sost* deletion. Here we show that conditional deletion of *Sost* in *Prx1*-expressing cells recapitulates the global high bone mass phenotype of *Sost*^{-/-}, resulting in ~250% more bone, in the femur. In contrast, both *Coll*- and *Dmp1*-specific deletions of *Sost* induced a significant but milder increase in bone formation, only 30% that of *Sost*^{-/-}, or ~80% more bone than wildtype (WT) controls. The vertebrae of *Prx1-Cre* deleted *Sost* mice also displayed a significant 50% increase in bone mass, suggesting that limb-bone derived sclerostin contributes significantly to the serum pool of sclerostin that normally suppresses bone formation in the spine. Moreover, the sclerostin produced in the axial skeleton (i.e., in the skeletal tissues that avoid *Prx1-Cre*-mediated recombination) is too dilute in the circulation to impair bone formation rates in the appendicular skeleton, where the *Sost* gene is recombined.

In addition, the relationships and interactions between the diverse cell types within the bone and their reciprocal effects on each other's cell fate decisions have become a focus of intense research, with clinical applications to improve bone fracture healing, prevent age-related bone loss and immune deficiencies. A significant knowledge gap exists as to the contribution of different osteolineage cells to the differentiation, proliferation, and long-term survival of B lymphocytes in the bone marrow (BM). In global sclerostin knockout (*Sost*^{-/-}) mice, we previously uncovered a cell-extrinsic requirement for sclerostin on B lymphocyte development⁽¹⁷⁾. Similar to mice with global *Sost* deletion, the total bone marrow cellularity in the femurs and tibiae was significantly reduced when *Sost* was deleted from *Prx1*-expressing cells. However, B lymphocyte development was differentially affected by *Sost* deletion in the *Prx1*-, *Coll*- and *Dmp1*-expressing cells, suggesting that a specific population of sclerostin-expressing cells in the bone influences B cell development and function.

Material and Methods

Experimental Animals

Mice with *C57Bl/6* background were used in this study. *Sost* conditional knockout (*Sost*^{*iCOIN/iCOIN*}) mice were generated by inserting an inverted GFP cassette, flanked by lox66 and lox71 sequences, in the intron of the *Sost* gene as previously described.⁽¹⁸⁾ Female mice with Cre under the *Prx1* promoter [B6.Cg-Tg(*Prrx1-cre*)1Cjt/J], *Coll* promoter [Tg(*Coll1a1-cre*)2Bek], *Dmp1* promoter [B6N.FVB-Tg(*Dmp1-cre*)1Jqfe/BwdJ], or *ColX* promoter [Tg(*Col10a1-cre*)1421Vdm] were mated to *Sost*^{*iCOIN/iCOIN*} male mice to generate conditional mutations in *Sost*^{*iCOIN/iCOIN*}; *Prx1-Cre*, *Sost*^{*iCOIN/iCOIN*}; *Coll-Cre*, *Sost*^{*iCOIN/iCOIN*}; *Dmp1-Cre* and *Sost*^{*iCOIN/iCOIN*}; *ColX-Cre* mice, respectively. Genotyping was completed by PCR. At 16 weeks of age, bones were dissected and processed for micro-computed tomography (μ CT), RNA,

histology and immunofluorescence (IF). All animal work was IACUC-approved and performed at Lawrence Livermore National Laboratory or UC Merced in AAALAC-accredited facilities.

Immunofluorescent Staining

Femur and lumbar vertebrae were collected at 16 weeks of age were fixed, dehydrated, embedded and sectioned as previously described.⁽⁵⁾ For immunofluorescence, Trypsin/EDTA was used for antigen retrieval for 25 minutes at 37°C. Primary antibodies: Anti-SOST (R&D, AF1589), Anti-GFP (Abcam, ab13970) and Anti-activated β -catenin (Millipore, Billerica, MA, USA) were used and incubated overnight at room temperature as previously described⁽¹⁹⁾. Negative control slides were incubated with secondary antibody-only. Stained slides were mounted with Prolong Gold with DAPI (Molecular Probes). ImagePro Plus V7.0 Software and a QIClick CCD camera were used for imaging and photo editing.

Micro-computed tomography

4th lumbar vertebrae and whole femora were collected and fixed for 48 hrs in 10% neutral buffered formalin, then stored in 70% EtOH at 4°C until scanning. The entire vertebra and the distal 60% of the femur were scanned on a Scanco uCT-35 specimen scanner using 60 kVp, 180 mA, 750 ms integration time, and 10 μ m voxel size⁽²⁰⁾. The entire cancellous region of the lumbar vertebra within 100 μ m of the endplates was isolated by manual analysis and included in the analysis. For the distal femur metaphysis, a 2-mm region of secondary spongiosa was isolated by manual analysis. The region of interest began 1 mm proximal to the distal growth plate and extended proximally for 2 mm. Prior to scanning, the total length of each femur was measured with digital calipers; these measurements were used to identify the mid-diaphysis slice in each femur CT scan by taking in to account slice thickness (10 μ m) and counting up in slices from the distal tip of the condyles until the calculated midshaft was reached. The central 20 slices at midshaft were analyzed for cortical properties.

Western Blot and Elisa

Femur and lumbar vertebrae were collected from 12-16 week old aged matched mice, frozen in liquid nitrogen and stored at -80°C until extraction. The bones were homogenized in 500 μ l of radioimmunoprecipitation assay buffer with appropriate volume of protease inhibitor cocktail (Sigma) at 1ml/20g tissue then incubated on ice for 20 minutes prior to centrifugation at 18,000g for 20 minutes at 4°C. The protein lysate supernatant was then quantified using BCA assay (Pierce) and stored at -80C. SDS-PAGE was performed with equal quantities of total protein per sample on Nupage protein gels

(ThermoFisher). Protein was then blotted onto a PVDF membrane (Licor) for western blot analysis. Membranes were probed with primary antibodies specific for Sost (AF1589, R&D Systems) and β -actin (926-42210, Licor) followed by IRDye 800CW donkey anti-goat and IRDye 680RD donkey anti-rabbit secondary antibodies. Membranes were then imaged using Licor Odyssey FC imaging system. Mouse sclerostin (ALPCO, 41-SCLMS-E01), Rankl (R&D Systems Cat#MTR00) and Ctx-1 ELISA kits (RatLaps EIA CTX-1 Cat# AC-06F1) were used according to the manufacturer's instructions (1:10 dilution for sclerostin and 1:1 dilution for Rankl and Ctx-1) to measure serum levels as previously described (N=3-4 per group) ⁽²¹⁾.

Bone Marrow Harvests

Mice were euthanized by CO₂ inhalation followed by cervical dislocation. Whole legs were dissected and muscles were removed. Bones were crushed with a mortar and pestle in Medium 199 containing 2% fetal calf serum (M199+) in order to release the bone marrow. BM cells were rinsed away from the bone chips with PBS and collected into 15 ml conical tubes, resuspended by trituration and filtered through 70 micron nylon mesh squares into sterile tubes. Cells were next washed with M199+ and centrifuged at 1500 rpm at 4°C for 5 minutes, after which cell pellets were resuspended and treated with ACK Lysis Buffer to remove erythrocytes. The ACK-treated cells were washed, resuspended in M199+ and total cell counts were obtained using a hemocytometer and Trypan Blue staining to exclude dead cells.

Analysis of Hematopoietic Cell Lineages by Flow Cytometry

The following antibodies were purchased from eBioscience or Biolegend: CD45 (30F11)-FITC, CD19 (6D5)-PE, GR1 (RB6-8C3)-PECy7, CD3 (145-2C11)-APC, CD11b (M1/70)-biotin, purified FcBlock CD16/32 (90), CD25 (PC61)-FITC, BP1 (Ly51/6C3)-PE, B220 (RA3-6B2)-PECy7, CD117 (2B8)-APC, Rat IgG2a-PE, kappa isotype control, CD19 (6D5)-FITC, CD43 (1B11)-PE, IgM-(eb121-15F9)-eFluor450, IgM (RMM01)-Brilliant Violet (BV) 421, IgD (11-26c.2a)- BV510. 1-2x10⁶ cells per sample were stained in 96-well V-bottom plates (Nunc, Inc) with their designated antibody cocktail and incubated for at least 15 min at 4°C before washing with FACS buffer and centrifuging at 2000 rpm at 4°C for 3 min. Supernatants were removed from the plates and cells incubated with streptavidin-Pacific Blue to develop biotinylated CD11b-stained cells when required. Cell viability was assessed using DAPI or propidium iodide (PI) solution at a final concentration of 0.2 μ g/ml. Cells were acquired on a Becton Dickinson LSR II and flow cytometric analysis was performed using FlowJo software.

Statistics

All data were expressed as the mean + standard deviation. For μ CT, and flow cytometry results, statistical analysis was done using Student's T-test with a two-tailed distribution, with two-sample equal variance (homoscedastic test) and one-way ANOVA with multiple comparisons. For all tests, $p < 0.05$ was considered statistically significant.

RESULTS

Dmp1-Cre Deletion Pattern Most Closely Recapitulates Endogenous Sost Expression, in Bone

Conditional deletion of *Sost* from different cell populations allows us to determine cell-specific contributions to bone metabolism as well as to distinguish local from systemic effects. Using a previously described *Sost* conditional loss-of-function by inversion allele (*Sost*^{*iCOIN/iCOIN*}),⁽¹⁸⁾ we eliminated *Sost* expression in (i) the limb mesenchyme (*Prx1-Cre*),⁽²²⁾ (ii) osteoblasts (*Coll-Cre*)⁽²³⁾; and (iii) osteocytes (*Dmp1-Cre*).⁽²⁴⁾ Upon Cre-mediated recombination, the conditional *Sost* allele undergoes premature termination of the endogenous *Sost* transcript, while simultaneously activating *eGFP* in frame with *Sost*, allowing us to track endogenous *Sost* expression using *eGFP* in cells that are now sclerostin deficient.⁽¹⁸⁾ Previously, it has been shown that a mouse of the *Sost*^{*iCOIN/LacZ*}; *LacZ*^{*Nannog-Cre/+*} genotype has high bone mass (HBM) indistinguishable from the global *Sost* knockout allele that replaces the *Sost* gene with the *LacZ* reporter (*Sost*^{*LacZ/LacZ*}; and referred to as *Sost*^{-/-} in this manuscript).^(5,18) Since the *iCOIN*-inverted allele allows us to visualize *Sost* deficient cells through the presence of *eGFP*, we first compared the *eGFP* expression in the bones of *Sost*^{*iCOIN/iCOIN*}; *Prx1-Cre*, *Sost*^{*iCOIN/iCOIN*}; *Coll-Cre*, *Sost*^{*iCOIN/iCOIN*}; *Dmp1-Cre* to the endogenous *Sost* expression in the control *Sost*^{*iCOIN/iCOIN*} mice.

Cortical bone expression of *eGFP* was highest in the osteocytes of *Dmp1-Cre* deleted mice, and punctate expression was also detected in the matrix, suggesting that the *Sost*-*eGFP* fusion protein is able to exit the osteocytes (Fig. 1A-D). Since *eGFP* is a membrane bound version, we speculate that this expression may be due to microvesicles shed by osteocytes. *Sost*^{*iCOIN/iCOIN*}; *Coll-Cre* deleted mice displayed the lowest expression levels in cortical osteocytes (Fig. 1C), suggesting that only a minority of embryonically labeled *Coll*-positive cell mature into osteocytes. In the trabecular region of the femurs, *Dmp1-Cre* mice also had the greatest expression; the expression was higher than the endogenous *Sost* expression (Fig 1A, D), suggesting that these cells are accumulating higher levels of *Sost*-*eGFP* than in the endogenous bone maybe due to retention of *eGFP* in the membrane (Fig. 1E-H). Similar to the cortical bone results, *Sost*^{*iCOIN/iCOIN*}; *Coll-Cre* mice also expressed *eGFP* in fewer trabecular osteocytes (Fig. 1G). The expression of *eGFP* in the vertebrae of *Sost*^{*iCOIN/iCOIN*}; *Coll-Cre* and *Sost*^{*iCOIN/iCOIN*}; *Dmp1-Cre* was

similar to that described above for the femoral trabeculae; however, consistent with its site of Cre recombinase expression, none of the *Sost*^{iCOIN/iCOIN}; *Prx1-Cre* mice did not express any eGFP in the vertebrae (Fig 1. I-L). Western blot analysis showed the highest Sost-eGFP and the lowest Sost expression in the *Sost*^{iCOIN/iCOIN}; *Prx1-Cre* femurs (Prx1), while no Sost-eGFP was detected in the vertebrae, consistent with *Prx1-Cre* site of expression in appendicular skeleton (Fig 1M). Sost serum levels were reduced by ~50% in *Prx1-Cre* mice, but no detectable Sost was measured in *Dmp1-Cre* and *Coll-Cre* mice (Fig 1N), this data suggests that Sost serum levels in *Prx1-Cre* mice is exclusively derived from the axial skeleton.

***Dmp1-Cre Deletion of Sost does not Recapitulate Sost*^{-/-} HBM Phenotype**

Originally, *Sost* was described as an osteocyte specific gene⁽²⁵⁾, and while in recent years *Sost* expression has been found in other organs and cell types of the skeleton⁽⁸⁾, osteocytes do express a robust amount of Sclerostin (Fig. fig 1A, E, I), therefore we anticipated that *Dmp1-Cre* deletion of *Sost* would most closely resemble the HBM phenotype of *Sost*^{-/-} mice. At 16 weeks of age, both *Sost*^{iCOIN/iCOIN}; *Coll-Cre* and *Sost*^{iCOIN/iCOIN}; *Dmp1-Cre* mice showed a significant increase in femoral BV/TV (Fig 2B, C, E-G), however, both these values were about 1/3 of those determined for *Sost*^{-/-} and *Sost*^{iCOIN/iCOIN}; *Prx1-Cre* mice, suggesting that both osteoblast- and osteocyte-specific deletion of *Sost* result in the same HBM phenotype (Fig 2G). Vertebral BV/TV was also significantly increased in *Sost*^{iCOIN/iCOIN}; *Coll-Cre* and *Sost*^{iCOIN/iCOIN}; *Dmp1-Cre* mice by 81% and 88%, respectively, or ~50% of HBM in *Sost*^{-/-} (Fig 2G).

***Prx1-Cre Deletion Recapitulates Sost*^{-/-} High Bone Mass Phenotype, in the Femur**

To determine whether conditional ablation of *Sost* in the limb mesenchyme, mature osteoblasts or osteocytes is sufficient to recapitulate the HBM phenotype observed in the *Sost*^{-/-} mice we also bred *Sost*^{iCOIN/iCOIN} mice to *Prx1-Cre*, in addition to *Coll-Cre* and *Dmp1-Cre* (Fig. 2 A–D). All conditional knockout mice were indistinguishable in size and weight from their same-sex Cre-negative control littermates. At 16 weeks of age, microscale computed tomography (μ CT) analysis of distal femurs showed that trabecular bone volume fraction (BV/TV) in all conditional knockouts was significant higher than the Cre-negative controls (Fig. 2a-d, E); however only the *Sost*^{iCOIN/iCOIN}; *Prx1-Cre* mice had a BV/TV increase of 257% (Table 1), a value similar to that of age matched *Sost*^{-/-} mice (+221%; Table 2), whereas both *Sost*^{iCOIN/iCOIN}; *Coll-Cre* and *Sost*^{iCOIN/iCOIN}; *Dmp1-Cre* mice had BV/TV increases of 85% and 81%, respectively (Fig. 2G; Table 1).

While *Sost*^{iCOIN/iCOIN}; *Prx1-Cre* femurs most closely resembled femurs from *Sost*^{-/-} mice, there were several noted differences. While *Sost*^{-/-} did not display a significant increase in trabecular number,

with only an 8% increase above wildtype, *Sost*^{iCOIN/iCOIN}; *Prx1-Cre* femurs had a significant 24.18% increase in trabecular number (Table 1, 2). Another significant difference was in the cortical values, where *Sost*^{iCOIN/iCOIN}; *Prx1-Cre* femurs did not display significant increases in either cortical bone volume but had a significant increase in cortical thickness; *Sost*^{-/-} had a significant 69.98% increase in cortical bone volume and a 31% increase in cortical BV/TV (Table 1, 2). Furthermore, neither *Sost*^{iCOIN/iCOIN}; *Dmp1-Cre* nor *Sost*^{iCOIN/iCOIN}; *Coll1-Cre* had a significant increase in cortical BV/TV despite a significant, but more modest increase in cortical bone volume (Table 1, 2). Lastly, cortical bone mineral density was unchanged in all conditional *Sost* mice, whereas *Sost*^{-/-} mice had a significant 3.21% gain (*p*-value=0.05) in cortical BMD (Table 1, 2). Consistent with the bone phenotype, levels of β -catenin were highest in the *Prx1-Cre* cortical and trabecular regions of the femur (Sup Fig 1).

Prx1-Cre Deletion Results in Increased Bone Formation, in the Vertebrae

Prx1-Cre drives Cre recombinase expression in uncommitted mesenchymal cells that contribute to bone, cartilage, muscle, white and brown adipose tissues of the developing appendicular skeleton. Cre is also expressed in portions of the skull, but absent from other parts of the axial skeleton.^(22,26) If *Sost* is retained locally, we anticipated *Prx1-Cre* deletion to cause HBM in the appendicular skeleton and to maintain normal bone mass in the axial skeleton, where *Sost* expression remains unperturbed. Lumbar vertebrae μ CT analysis between *Sost*^{iCOIN/iCOIN}; *Prx1-Cre* and age-matched *Sost*^{iCOIN/iCOIN} control mice uncovered a significant (55%) increase in BV/TV ratio, suggesting that lack of *Sost* in the appendicular skeleton positively affects bone formation in the vertebrae (Fig. 2aa, F, G, Table 1). While trabecular number was not different in *Sost*^{iCOIN/iCOIN}; *Prx1-Cre* than controls, the trabecular thickness was significantly elevated by 16%. In addition, the trabecular bone mineral content was elevated by 88%, half of the *Sost*^{-/-} value. Interestingly, neither *Coll1-Cre* nor *Dmp1-Cre* deletion of *Sost* resulted in BV/TV increases similar to those measured for *Sost*^{-/-}; displaying 81% and 88% increase, about half of *Sost* values (Fig. 2bb, cc, dd, F, G; Table 1,2).

Prx1-Cre Deletion of Sost Results in Reduced Bone Marrow Cellularity

To determine which *Sost*-expressing osteolineage cell type is responsible for B lymphocyte support, we analyzed hematopoietic differentiation in mice lacking *Sost* specifically in osteoprogenitors/MSCs [*Prx1-Cre*], osteoblasts [*Coll1a-Cre*] and osteocytes [*Dmp1-Cre*]. Similar to the global *Sost*^{-/-} mouse, *Sost*^{iCOIN/iCOIN}; *Prx1-Cre* mice displayed a significant reduction in total BM cellularity; however, deletion of *Sost* in osteoblasts and osteocytes had no effect (Fig. 3B). We further examined the frequency (%) and absolute number of total CD19⁺ B cells, and observed that the % of CD19⁺ cells was slightly reduced

when *Sost* was deleted in osteoblasts and osteocytes (Fig. 3A, C), but the absolute numbers of CD19+ cells were significantly reduced in the *Sost^{iCOIN/iCOIN}; Prx1-Cre* and *Sost^{iCOIN/iCOIN}; Coll-Cre* mice only (Fig. 3D).

The CD19+ B cell population in the BM contains a heterogeneous mixture of B cell progenitors, developing B cells and mature B cells, which can be distinguished by expression of B220 and diminishing levels of CD43 (Fig. 4A and Sup Fig. 2A and Hardy et al⁽²⁷⁾). B220+ CD43^{high} cells are B cell progenitors with low expression of surface IgM and IgD. The B220+ CD43-intermediate (B220+ CD43^{int}) population begin to express surface IgM and coexpression of IgD can be observed as cells progress to the B220+ CD43^{low} population. Finally, the B220+ CD43-negative (B220+ CD43^{neg}) population is the most mature B cell population, displaying high levels of IgM and IgD. In order to determine if the four specific B cell stages and the transition from one stage to the next were differentially affected by *Sost* deletion in specific osteolineage cell types, we enumerated the % and absolute numbers of B cells within each B220/CD43 subset, and their expression of IgM and IgD receptors in the conditional *Sost* knockout mouse strains. In the global *Sost* knockdown, knockout, a developmental block beginning at the pre-B stage (similar to Hardy Fractions B and C⁽²⁷⁾) and all committed B cell stages were observed⁽¹⁷⁾ with changes in both frequency and cell number. Our analysis of the *Sost^{iCOIN/iCOIN}; Prx1-Cre* bone marrow showed an increase in the % of phenotypically mature B220+ CD43^{neg} cells compared to no Cre controls (Fig. 4B). In contrast, the % of B220+ CD43^{neg} cells was significantly decreased in the *Sost^{iCOIN/iCOIN}; Dmp1-Cre* bone marrow. This suggested that deletion of *Sost* in the MSCs resulted in expansion of mature B cells, whereas deletion of *Sost* in the osteocytes resulted in fewer mature B cells. However, the absolute numbers of B220+ CD43^{neg} cells were not affected (Sup Fig. 3). Mature B cells should express high levels of IgM and IgD. Examination of IgM and IgD expression in the mature B cells of the *Sost^{iCOIN/iCOIN}; Prx1-Cre* bone marrow revealed an abnormally high proportion of cells that lacked expression of both IgM and IgD (Fig. 4F and Sup Fig. 2B). In line with this, the *Sost^{iCOIN/iCOIN}; Prx1-Cre* mice displayed the lowest proportion of mature IgM+ IgD+ cells amongst the different mouse strains (Fig. 4F). Closer examination of the immature B220+ CD43^{int}-subset showed a similar trend of higher % of IgM- IgD- and lower % of IgM+ IgD^{low} cells in the *Sost^{iCOIN/iCOIN}; Prx1-Cre* bone marrow (Fig. 4E). These results indicate that deletion of *Sost* in the *Prx1+* cells affects upregulation of IgM and IgD at the later stages of B cell maturation.

We also observed changes in B cell maturation in the *Sost^{iCOIN/iCOIN}; Coll-Cre* bone marrow, but in contrast to the *Prx1-Cre* bone marrow, the progenitor and early stages of development were altered. Significantly higher proportions of IgM- IgD- cells were observed at the B220+ CD43^{high} and B220+ CD43^{int} subsets. This article is protected by copyright. All rights reserved

CD43^{int} stages (Fig. 4C and 4D), as well as lower proportion IgM⁺ IgD^{low} cells. This suggested that the progression of B cells from the progenitor to early stages of development was somewhat delayed, and could explain the increased proportion of immature B220⁺ CD43^{low} cells in the *Sost*^{COIN/COIN}; *Coll-Cre* bone marrow (Fig. 4B) and lower % and number of IgM⁺ IgD⁺ cells within this subset compared to the other mouse strains (Fig. 4E and Sup Fig. 2C and 3C). Despite these changes, the proportions and numbers of mature B220⁺ CD43^{neg} were similar to no Cre controls (Fig. 4F and Sup Fig. 3D). Results from analysis of B cell subsets using alternative staining strategies were consistent with these results (data not shown). B cell development in *Sost*^{COIN/COIN}; *Dmp1-Cre* bone marrow was not significantly altered at any stage (Fig. 4C-F). These data suggest that *Prx1-Cre* and *Coll-Cre*, but not *Dmp1-Cre* deletion removes sclerostin in a subtype of osteoprogenitors required for distinct stages of B cell development.

ColX-Cre Deletion of Sost Results in High Bone Mass

ColX-Cre drives Cre recombinase expression in hypertrophic chondrocytes, cells that recently have been shown to trans-differentiate into osteoblasts.^(29,30) Using lineage tracing, it has been shown that *ColX*-positive cells substantially participate in trabecular, endosteal and cortical bone formation.⁽²⁹⁾ To determine whether conditional ablation of *Sost* in these cells also affects bone mass we compared *ColX-Cre* conditional knockouts to the Cre-negative littermates. Microcomputed tomography (μ CT) analysis of distal femurs showed that *Sost*^{COIN/COIN}; *ColX-Cre* knockouts had a significant 37.57% increase in the femoral and a 22.71% increase in the vertebral trabecular bone volume fractions (BV/TV) relative to the Cre negative controls (Table 3). Cortical bone mineral content was slightly elevated, but no other cortical parameters were significantly different, suggesting that *ColX-Cre* ablates *Sost* from a unique population of osteoprogenitor cells that give rise to *Sost* positive cells, in the adult bone. LacZ staining of mice carrying a *Sost-LacZ* allele did not detect *Sost/LacZ* expression in the hypertrophic chondrocytes of neonatal mice (Sup Fig. 4C), suggesting that the high bone mass phenotype is due to a subpopulation of *Sost* deficient osteoblasts and osteocytes, primarily in the trabecular compartment.

Discussion:

Sost/sclerostin is highly expressed in the osteocyte population (Sup Fig4A, B), and thus it has been hypothesized that the phenotypes observed in bone and hematopoietic development when *Sost* is deleted were due to lack of *Sost* in the osteocytes. Contrary to this assumption, *Dmp1-Cre* deletion did not recapitulate the global *Sost* phenotype, unlike *Prx1-Cre* which fully recapitulated the *Sost* global phenotype in the appendicular skeleton. This result can have several interpretations: either *Dmp1-Cre* is incapable of ablating the *Sost* allele in all *Sost*-expressing osteocytes, and the residual non-recombined

This article is protected by copyright. All rights reserved

osteocytes express sufficient *Sost* to blunt the otherwise strong phenotype locally, or several distinct populations of cells in the bone express *Sost*, and all these cells are derived from *Prx1*-positive progenitors. The interpretation that other cell types in addition to osteocytes are important contributors to the local pool of Sclerostin protein in bone is further supported by the observation that *Coll1-Cre* deletion of *Sost* also had a HBM phenotype, but significant differences were noted between *Coll1* and *Dmp1* deletions. For example, a significant difference was observed in the femoral cortical thickness, where *Dmp1* deletion did not increase the cortical thickness, but both *Coll1* and *Prx1* did, implying that a subpopulation of periosteal osteoblasts do express *Sost* and these cells could be a population of osteochondral progenitors as previously suggested by Quyang et al⁽³¹⁾.

Since only *Prx1-Cre* deletion of *Sost* recapitulates the HBM phenotype of *Sost* global knockout, in the appendicular skeleton, we can conclude that the only *Sost* expression affecting bone mass is derived from descendants of *Prx1*-positive limb bud progenitors (Fig. 5). During embryonic development *Prx1*-positive mesenchymal stem cells (MSC) give rise to muscle, adipocyte and osteochondral progenitors, which are the predecessors of mature myocytes, adipocytes, chondrocytes, hypertrophic chondrocytes, osteoblasts and osteocytes. While endogenous *Prx1* is also expressed in the vertebrae and is required for early events of skeletogenesis in multiple lineages⁽³²⁾, the *Prx1-Cre* transgene expresses Cre recombinase from a limb enhancer, therefore, the *Cre* expression is restricted to all limb bud MSC derived cells of the appendicular skeleton⁽²²⁾. Here we showed that *Sost* deletion in mature osteoblasts and their descendant (*Coll1-Cre*) or mature osteocytes (*Dmp1-Cre*) elevate bone mass by 80%, respectively, while deletion in hypertrophic chondrocytes and their descendants (*ColX-Cre*) elevated trabecular bone mass by 37%. While all these individual alleles do have a significant HBM phenotype, none does, nor do they all cumulatively sum up to the HBM amplitude of *Prx1-Cre* or *Sost*^{-/-} alleles (80%+80%+37.5% < 250% BV/TV; Tables 1-3), further strengthening the argument that additional *Prx1*-derived cells are responsible for *Sost* expression, in bone. The two lineages not represented in our collection of *Cre* alleles are the myogenic and the adipogenic lineages which cannot yet be excluded as contributors to both the HBM and the B cell phenotypes. Mining available microarrays and RNA-seq data sets did not identify significant transcript levels of *Sost* in other *Prx1* derived cell types, however, future improvements in cell purification methods followed by RNA-seq may identify subpopulations of cell expressing *Sost*. *Sost* expression has also been observed in the osteoclasts of aging mice⁽³³⁾; while we did not examine the phenotype of osteoclast-specific deletion of *Sost*, global *Sost* knockout, nor any of the conditional strains examined showed a significant change in markers of resorption (Sup Fig. 5).

Herein, we have also presented data that emphasizes novel roles for sclerostin in MSCs and OBs which distinctly impact BM cellularity and B cell maturation, and we conclude that loss of *Sost* in mature
This article is protected by copyright. All rights reserved

osteocytes does not play a major role in regulating B cell development. Loss of *Sost* expression in *Prx1*-positive MSCs and their descendants resulted in reduced BM cellularity, whereas this process was unaffected by *Sost*-deficiency in mature osteoblasts (*Col1-Cre*) and osteocytes (*Dmp1-Cre*). Furthermore, MSC-specific depletion of *Sost* caused an accumulation of abnormal B cells with no or low expression of IgM and IgD receptors that otherwise appeared phenotypically mature. The changes observed in the frequencies and the absolute numbers of B cell subsets did not follow the same patterns. For example, the % of of progenitors, early, immature and mature B cell subsets increased or decreased amongst the different deleter strains, but their numbers were not significantly different among all groups (Fig. 4B and Sup Fig. 3). This may stem from the fact that MSCs, osteoblasts, and osteocytes have a progenitor-progeny relationship and it is likely that deletion of *Sost* in each cell type is not synchronized, so some MSCs may progress to the osteoblast stage before *Sost* deletion occurs and support B cell development normally. Since total BM cellularity is decreased in the *Prx1-Cre* mice, one might expect that the cell number in all fractions would be proportionally decreased; however, only numbers of B220⁺ CD43^{int} immature were significantly reduced when *Sost* was deleted in MSCs, indicating that immature B cells require normal *Sost* levels. Our findings are consistent with recent work that demonstrated that MSCs and osteoblasts are important “niche cells” for early B cell development, with respect to their production of CXCL12^(34,35). CXCL12 expression is regulated by Wnt signaling in BM stromal cells *in vitro*.⁽³⁶⁾ We observed diminished CXCL12 levels in non-hematopoietic cells of the bone in and correlated the diminished CXCL12 levels with the reduction in B cell development in the global *Sost*^{-/-} mice.⁽¹⁷⁾ Our present results suggest that *Sost* specifically expressed in MSCs and osteoblasts regulate B cell development, but further analysis is required to determine if expression of CXCL12 and other Wnt target genes are altered in MSCs and osteoblasts in the *Prx1-Cre* and *Col1-Cre Sost* deleters.

Alternatively, it is possible that the B cell defect is indirect. Recently we have observed that bone marrow adiposity positively correlates with *Sost* expression levels, such that a mouse model of type I diabetes mellitus (T1DM) with elevated levels of *Sost* displayed enhanced bone marrow adiposity and this phenotype was rescued by *Sost* antibody treatment.⁽²¹⁾ Also, a recent report has described Sclerostin as a promoter of adipogenic differentiation⁽³⁷⁾ suggesting that lack of *Sost* may impair adipogenesis. Bone marrow adipocytes can be lineage-traced using *Prx1-Cre* and *Osx-Cre*, in contrast to other adipocyte lineages⁽³⁸⁾, and the microenvironment in the bone marrow of aged mice appears to favor adipogenesis over osteogenesis in mesenchymal progenitor cells⁽³⁹⁾. The relationship between adipocytes and immune cell development is a current area of research. The transition of human common lymphocyte progenitors to the early pre-proB cell stages have been shown to be inhibited by a soluble factor produced by bone marrow adipocytes⁽⁴⁰⁾, and stem cell factor produced by Lepr⁺ BM adipocyte precursors is necessary for

This article is protected by copyright. All rights reserved

the generation of B cells and other hematopoietic cells in mice⁽⁴¹⁾. Based on these data, any impairment in adipogenesis by *Sost* depletion may be unrelated to the decrease in mature B cells we have observed in *Sost*-knockout mice. Nonetheless, it would be worth exploring whether *Sost* affects B cell development by interfering with bone marrow adipogenesis. Our analysis of global *Sost* knockout mice showed significant decreases in the B cell precursors and immature subsets but this was not as dramatic in the *Sost*^{iCOIN/iCOIN}; *Prx1-Cre* mice, which suggests that there is another cell that expresses *Sost* that is important in supporting these early B cell subsets. In contrast, *Prx1*⁺ and *Col1*⁺ *Sost*-expressing cells are critical for normal B cell maturation. It remains to be determined whether the bone marrow adipocytes in these *Sost*-deficient mice are reduced or impaired in their function to support B cell maturation.

Our analyses demonstrate that deletion of *Sost* in mature osteocytes does not significantly impair B lymphocyte development nor does it cause the HBM observed in the global *Sost*^{-/-} therefore other cell types derived from *Prx1*-positive MSCs are critical in these processes. Furthermore, we show that *Prx1-Cre* deletion of *Sost* resulted in a significant increase in bone mass in the axial skeleton, where *Sost* alleles remain wildtype. This result suggests that *Sost* expressed in the vertebra is diluted out in the circulation, decreasing the net pool of *Sost* in the axial skeleton and contributing the increased BV/TV in this tissue, however, the vertebra derived *Sost* in circulation does not act in an endocrine fashion, leaving the appendicular skeleton unperturbed. These results indicate that *Sost* primarily acts locally in bone *via* paracrine secretion and that endocrine secretion of *Sost* from distant sites do not significantly impair bone mass. Since anti-sclerostin antibodies are likely to become a new therapy to build bone in osteoporosis patients, it is imperative to target these therapies to bone to avoid undesired side-effects in other tissues that may require *Sost* for their proper function, and to test whether these therapies leave B cell development unperturbed in these patients. Our results suggest that if *Sost*-depletion by *Sost* antibodies is limited to osteocytes, possible side effects on B cell development and immunity could be avoided, but may elicit a more modest anabolic effect on bone mass.

Author Contributions

GGL and JOM designed research. CSY, JOM, JC, NRH, MEM and DKM performed research. AEE generated and provided the *Sost*^{iCOIN} allele. AGR and DJH performed microCT scans and analysis. GGL and JOM analyzed data. CSY, JOM and GGL wrote the paper.

Acknowledgements

This work was performed under the auspices of the U.S. Department of Energy by Lawrence Livermore National Laboratory under Contract DE-AC52-07NA27344. CSY, JC, NRH, DKM and GGL were supported in part by NIH Grants RO1 DK075730 and R56 DK110145. JOM was funded by the University of California. We thank the staff in the Department of Animal Research Services at UC Merced and at LLNL for excellent mouse care.

Accepted Article

References

1. Baron R, Kneissel M. WNT signaling in bone homeostasis and disease: from human mutations to treatments. *Nat Med. Research Support, N.I.H., Extramural Review* Feb 2013;19(2):179-92. Epub 2013/02/08.
2. Atkins GJ, Rowe PS, Lim HP, Welldon KJ, Ormsby R, Wijenayaka AR, et al. Sclerostin is a locally acting regulator of late-osteoblast/preosteocyte differentiation and regulates mineralization through a MEPE-ASARM-dependent mechanism. *J Bone Miner Res.* Jul 2011;26(7):1425-36.
3. Balemans W, Ebeling M, Patel N, Van Hul E, Olson P, Dioszegi M, et al. Increased bone density in sclerosteosis is due to the deficiency of a novel secreted protein (SOST). *Hum Mol Genet.* Mar 1 2001;10(5):537-43. Epub 2001/02/22.
4. Brunkow ME, Gardner JC, Van Ness J, Paepfer BW, Kovacevich BR, Proll S, et al. Bone dysplasia sclerosteosis results from loss of the SOST gene product, a novel cystine knot-containing protein. *Am J Hum Genet.* Mar 2001;68(3):577-89. Epub 2001/02/17.
5. Collette NM, Genetos DC, Economides AN, Xie L, Shahnazari M, Yao W, et al. Targeted deletion of Sost distal enhancer increases bone formation and bone mass. *Proc Natl Acad Sci U S A.* Aug 10 2012. Epub 2012/08/14.
6. Li X, Ominsky MS, Niu QT, Sun N, Daugherty B, D'Agostin D, et al. Targeted deletion of the sclerostin gene in mice results in increased bone formation and bone strength. *J Bone Miner Res.* Jun 2008;23(6):860-9.
7. Loots GG, Kneissel M, Keller H, Baptist M, Chang J, Collette NM, et al. Genomic deletion of a long-range bone enhancer misregulates sclerostin in Van Buchem disease. *Genome Res.* Jul 2005;15(7):928-35.
8. Collette NM, Yee CS, Murugesu D, Sebastian A, Taher L, Gale NW, et al. Sost and its paralog Sostdc1 coordinate digit number in a Gli3-dependent manner. *Dev Biol.* Nov 01 2013;383(1):90-105.
9. Winkler DG, Sutherland MK, Geoghegan JC, Yu C, Hayes T, Skonier JE, et al. Osteocyte control of bone formation via sclerostin, a novel BMP antagonist. *Embo J.* Dec 1 2003;22(23):6267-76. Epub 2003/11/25.
10. Jastrzebski S, Kalinowski J, Stolina M, Mirza F, Torreggiani E, Kalajzic I, et al. Changes in bone sclerostin levels in mice after ovariectomy vary independently of changes in serum sclerostin levels. *J Bone Miner Res. Research Support, N.I.H., Extramural Research Support, Non-U.S. Gov't* Mar 2013;28(3):618-26. Epub 2012/10/10.
11. Ardawi MS, Al-Kadi HA, Rouzi AA, Qari MH. Determinants of serum sclerostin in healthy pre- and postmenopausal women. *J Bone Miner Res.* Dec 2011;26(12):2812-22. Epub 2011/08/04.
12. Ardawi M-SM, Al-Kadi HA, Rouzi AA, Qari MH. Determinants of Serum Sclerostin in Healthy Pre- and Postmenopausal Women. *Journal of Bone and Mineral Research.* 2011;26(12):2812-22.
13. Mirza FS, Padhi ID, Raisz LG, Lorenzo JA. Serum sclerostin levels negatively correlate with parathyroid hormone levels and free estrogen index in postmenopausal women. *J Clin Endocrinol Metab. Research Support, Non-U.S. Gov't* Apr 2010;95(4):1991-7. Epub 2010/02/17.

14. Fujita K, Roforth MM, Demaray S, McGregor U, Kirmani S, McCready LK, et al. Effects of estrogen on bone mRNA levels of sclerostin and other genes relevant to bone metabolism in postmenopausal women. *J Clin Endocrinol Metab. Randomized Controlled Trial Research Support, N.I.H., Extramural* Jan 2014;99(1):E81-8. Epub 2013/10/31.
15. Fujita K, Roforth MM, Demaray S, McGregor U, Kirmani S, McCready LK, et al. Effects of Estrogen on Bone mRNA Levels of Sclerostin and Other Genes Relevant to Bone Metabolism in Postmenopausal Women. *The Journal of Clinical Endocrinology and Metabolism.* 2014;99:E81-E8.
16. Chung YE, Lee SH, Lee SY, Kim SY, Kim HH, Mirza FS, et al. Long-term treatment with raloxifene, but not bisphosphonates, reduces circulating sclerostin levels in postmenopausal women. *Osteoporos Int. Research Support, Non-U.S. Gov't* Apr 2012;23(4):1235-43. Epub 2011/06/11.
17. Cain CJ, Rueda R, McLelland B, Collette NM, Loots GG, Manilay JO. Absence of sclerostin adversely affects B cell survival. *J Bone Miner Res.* Mar 20 2012. Epub 2012/03/22.
18. Economides AN, Friendewey D, Yang P, Dominguez MG, Dore AT, Lobov IB, et al. Conditionals by inversion provide a universal method for the generation of conditional alleles. *Proc Natl Acad Sci U S A.* Aug 20 2013;110(34):E3179-88. Epub 2013/08/07.
19. Chang JC, Christiansen BA, Muruges DK, Sebastian A, Hum NR, Collette NM, et al. SOST/Sclerostin Improves Post Traumatic Osteoarthritis and Inhibits MMP2/3 Expression After Injury. *J Bone Miner Res.* Jan 26 2018. Epub 2018/01/30.
20. Bouxsein ML, Boyd SK, Christiansen BA, Guldberg RE, Jepsen KJ, Muller R. Guidelines for assessment of bone microstructure in rodents using micro-computed tomography. *J Bone Miner Res.* Jul 2010;25(7):1468-86. Epub 2010/06/10.
21. Yee CS, Xie L, Hatsell S, Hum N, Muruges D, Economides AN, et al. Sclerostin antibody treatment improves fracture outcomes in a Type I diabetic mouse model. *Bone.* Jan 2016;82:122-34.
22. Logan M, Martin JF, Nagy A, Lobe C, Olson EN, Tabin CJ. Expression of Cre Recombinase in the developing mouse limb bud driven by a Prxl enhancer. *Genesis. Research Support, Non-U.S. Gov't* Research Support, U.S. Gov't, P.H.S. Jun 2002;33(2):77-80. Epub 2002/07/12.
23. Liu F, Woitge HW, Braut A, Kronenberg MS, Lichtler AC, Mina M, et al. Expression and activity of osteoblast-targeted Cre recombinase transgenes in murine skeletal tissues. *Int J Dev Biol.* Sep 2004;48(7):645-53. Epub 2004/10/08.
24. Lu Y, Xie Y, Zhang S, Dusevich V, Bonewald LF, Feng JQ. DMP1-targeted Cre expression in odontoblasts and osteocytes. *J Dent Res.* Apr 2007;86(4):320-5. Epub 2007/03/27.
25. van Bezooijen RL, ten Dijke P, Papapoulos SE, Lowik CW. SOST/sclerostin, an osteocyte-derived negative regulator of bone formation. *Cytokine Growth Factor Rev.* Jun 2005;16(3):319-27. Epub 2005/05/05.
26. Krueger KC, Costa MJ, Du H, Feldman BJ. Characterization of Cre recombinase activity for in vivo targeting of adipocyte precursor cells. *Stem cell reports. Research Support, N.I.H., Extramural* Research Support, Non-U.S. Gov't Dec 9 2014;3(6):1147-58. Epub 2014/12/03.
27. Hardy RR, Carmack CE, Shinton SA, Kemp JD, Hayakawa K. Resolution and characterization of pro-B and pre-pro-B cell stages in normal mouse bone marrow. *J Exp Med.* May 01 1991;173(5):1213-25.
28. Khass M, Buckley K, Kapoor P, Schelonka RL, Watkins LS, Zhuang Y, et al. Recirculating bone marrow B cells in C57BL/6 mice are more tolerant of highly hydrophobic and highly charged

- CDR-H3s than those in BALB/c mice. *Eur J Immunol. Research Support, N.I.H., Extramural* Mar 2013;43(3):629-40. Epub 2012/12/12.
29. Park J, Gebhardt M, Golovchenko S, Perez-Branguli F, Hattori T, Hartmann C, et al. Dual pathways to endochondral osteoblasts: a novel chondrocyte-derived osteoprogenitor cell identified in hypertrophic cartilage. *Biol Open. Apr 16 2015;4(5):608-21.*
30. Yang L, Tsang KY, Tang HC, Chan D, Cheah KS. Hypertrophic chondrocytes can become osteoblasts and osteocytes in endochondral bone formation. *Proc Natl Acad Sci U S A. Aug 19 2014;111(33):12097-102.*
31. Ouyang Z, Chen Z, Ishikawa M, Yue X, Kawanami A, Leahy P, et al. Prx1 and 3.2kb Col1a1 promoters target distinct bone cell populations in transgenic mice. *Bone. Oct 25 2013.*
32. Martin JF, Bradley A, Olson EN. The paired-like homeo box gene MHOX is required for early events of skeletogenesis in multiple lineages. *Genes Dev. May 15 1995;9(10):1237-49. Epub 1995/05/15.*
33. Ota K, Quint P, Ruan M, Pederson L, Westendorf JJ, Khosla S, et al. Sclerostin is expressed in osteoclasts from aged mice and reduces osteoclast-mediated stimulation of mineralization. *J Cell Biochem. Aug 2013;114(8):1901-7. Epub 2013/03/16.*
34. Ding L, Morrison SJ. Haematopoietic stem cells and early lymphoid progenitors occupy distinct bone marrow niches. *Nature. Research Support, N.I.H., Extramural Research Support, Non-U.S. Gov't Mar 14 2013;495(7440):231-5. Epub 2013/02/26.*
35. Sellers WF, Yogendran S. Difficult tracheal intubation. *Anaesthesia. Case Reports Letter Nov 1987;42(11):1243. Epub 1987/11/01.*
36. Tamura M, Sato MM, Nashimoto M. Regulation of CXCL12 expression by canonical Wnt signaling in bone marrow stromal cells. *The international journal of biochemistry & cell biology. Research Support, Non-U.S. Gov't May 2011;43(5):760-7. Epub 2011/02/08.*
37. Ukita M, Yamaguchi T, Ohata N, Tamura M. Sclerostin Enhances Adipocyte Differentiation in 3T3-L1 Cells. *J Cell Biochem. Jun 2016;117(6):1419-28.*
38. Horowitz MC, Berry R, Holtrup B, Sebo Z, Nelson T, Fretz JA, et al. Bone marrow adipocytes. *Adipocyte. Aug 24 2017:1-12.*
39. Singh L, Brennan TA, Russell E, Kim JH, Chen Q, Brad Johnson F, et al. Aging alters bone-fat reciprocity by shifting in vivo mesenchymal precursor cell fate towards an adipogenic lineage. *Bone. Apr 2016;85:29-36.*
40. Bilwani FA, Knight KL. Adipocyte-derived soluble factor(s) inhibits early stages of B lymphopoiesis. *J Immunol. Nov 01 2012;189(9):4379-86.*
41. Zhou BO, Yu H, Yue R, Zhao Z, Rios JJ, Naveiras O, et al. Bone marrow adipocytes promote the regeneration of stem cells and haematopoiesis by secreting SCF. *Nat Cell Biol. Aug 2017;19(8):891-903.*
42. Collette NM, Genetos DC, Muruges D, Harland RM, Loots GG. Genetic evidence that SOST inhibits WNT signaling in the limb. *Dev Biol. Jun 15 2010;342(2):169-79.*

Figure Legends:

Fig. 1. Evaluating Efficiency of *Sost* conditional deletion in bone. Endogenous *Sost* protein expression in *Sost*^{iCOIN/iCOIN} was visualized in cortical and trabecular bone of the femur (A, E) and vertebrae (I) by immunohistochemistry and was consistent with previous wildtype expression of *Sost* (red) in mice (blue DAPI). Cre deletion of *Sost* allele activates eGFP, *Sost* expressing cells and carrying *Sost* deletion now express a *Sost*-eGFP fusion protein which is visualized in panels B, C, D, F, G, H, J, K, L in red; blue DAPI). *Prx1-Cre* deletion activated eGFP in *Sost* deficient cortical (B), and trabecular osteocytes (F) in the femur, but not in the vertebrae, where *Prx1-Cre* is not expressed (J). *Coll-Cre* deletion activated eGFP in *Sost* deficient cortical (C), and trabecular osteocytes (G) in the femur, and also in the osteocytes within the vertebrae (K). *Dmp1-Cre* deletion activated eGFP in *Sost* deficient cortical (D), and trabecular osteocytes (H) in the femur, and also in the osteocytes within the vertebrae (L). Western blot analysis (M) showed that most of *Sost* expression was removed in *Prx1*, *Coll1* and *Dmp1* deleted femurs, but *Sost* expression persisted in the *Prx1* vertebrae. eGFP protein expression inversely correlated with the *Sost* expression (M).

Fig. 2. Comparing Skeletal Phenotypes of *Sost* conditional mice to *Sost*^{-/-} mice. MicroCT analysis of axial and appendicula skeleton of *Prx1-Cre* (A), *Coll-Cre* (B), *Dmp1-Cre* and *Sost*^{-/-} (D) visually highlights increases in bone mass in both femurs (a, b, c, d) and vertebrae (aa, bb, cc, dd). *Prx1-Cre* deletes *Sost* in all MSC-derived cells in the appendicular skeleton only (A, red); *Coll-Cre* (B) and *Dmp1-Cre* (C) delete *Sost* in osteoblast and osteocytes throughout the skeleton; global knockout deletes *Sost* in all cell types of the skeleton (D). Quantification of trabecular BV/TV finds all mice to have a significant increase in both the femoral (E) and vertebral (F) bone fractions, however, only *Prx1-Cre* mice had a % change in BV/TV comparable to *Sost*^{-/-} (G). **p*<0.05, both by ANOVA and t-test.

Fig. 3. Bone marrow cellularity and lymphocyte frequencies and cell numbers are differentially affected by the absence of *Sost* in specific osteolineage cell types. A) Representative flow cytometry plots of CD19 (B cell) and CD3 (T cell) lineages in the bone marrow of no-Cre control and conditional *Sost* knockout mice (A); Total bone marrow cellularity (B); Frequencies of CD19+ cells out of total BM cells (C); Absolute numbers of CD19+ B cells in BM (D). **p*<0.05, ***p*<0.01, ****p*<0.001 both by ANOVA and t-test, except in B, where comparison of control vs. *Prx1-Cre* by ANOVA showed *p*<0.01, and C, where comparison of control vs. *Coll-Cre* by ANOVA showed *p*<0.05.

Fig. 4. Loss of *Sost* in MSCs and OBs differentially regulates earlier and later stages of B cell development in the bone marrow. A) Schematic of B lineage maturation in the bone marrow, with cell surface markers for each maturation stage indicated. B) Stacked bar graph of mean frequencies + standard deviation of progenitor (pro-B/pre-B, black) early (light green), immature (grey) and mature (yellow) B cell stages, and mean frequencies + standard deviation of IgM- IgD- (red), IgM+ IgD^{low} (blue), and IgM+ IgD+ (beige) in C) pro-B/pre-B, D) early, E) immature and F) mature B cells stages in control (no Cre), *Prx1-Cre*, *Coll-Cre*, and *Dmp1-Cre* conditional *Sost* knockout mice. * $p < 0.05$, Student's t-test. Exact p -values for comparisons of interest that did not achieve $p < 0.05$ are shown in the stacked bar corresponding to the group.

Fig. 5. Cell types along the MSC/*Prx1-Cre* lineages. *Prx1-Cre* deletes early during differentiation and ablates *Sost* in all derived cells, this mouse fully recapitulates the *Sost*^{-/-} phenotypes. *Coll-Cre* and *Dmp1-Cre* ablate *Sost* in the osteoblast lineage, and both deletions result in similar phenotypes. *ColX-Cre* ablates *Sost* in the hypertrophic chondrocytes, and has the lowest increase in BM.

Supplementary Fig. 1. Activated β -catenin in conditional *Sost* knockout mice. Cortical (A-F) and trabecular (a-f) regions of the femur were examined for β -catenin expression in no *Cre* wildtype controls (A, a) global *Sost* knockout (B, b) and conditional knockouts *Sost*^{iCOIN/iCOIN}; *Prx1-Cre* (C, c), *Sost*^{iCOIN/iCOIN}; *Col1-Cre* (D, d), *Sost*^{iCOIN/iCOIN}; *Dmp1-Cre* (E, e) and *Sost*^{iCOIN/iCOIN}; *ColX-Cre* (F, f). *bm* bone marrow, *t* trabecular.

Supplemental Fig. 2. Examples of flow cytometry analysis of B cell maturation in conditional *Sost* knockout mice. A) scheme of B cell maturation and flow cytometry “map” of the subsets in plots shown in B and C. B) representative plots of bone marrow from a “no *Cre*” control and 2 *Sost*^{iCOIN/iCOIN}; *Prx1-Cre* mice; C) representative plots from a “no *Cre*” control, and a *Sost*^{iCOIN/iCOIN}; *Col1-Cre* and a *Sost*^{iCOIN/iCOIN}; *Dmp1-Cre* mouse.

Supplemental Fig. 3. Absolute cell counts amongst B cell subsets in conditional *Sost* knockouts. A) # of cells by maturation stage as defined by B220 and CD43 expression. Analysis of IgM-IgD⁻, IgM+ IgD^{low} and IgM+ IgD⁺ cells within B) early, C) immature and D) mature stages of B cell development. No differences in cell counts were observed amongst the pro-B/pre-B subsets (data not shown). **p*<0.05, unpaired Student’s t-test.

Supplementary Fig. 4. LacZ expression in *Sost* knockouts with LacZ knock-in. *Sost*^{-/-} mice with the *LacZ* reporter, which were previously described⁽⁴²⁾, were collected and stained as previously described⁽⁸⁾. *Sost* expression in adult was detected in the osteocytes within bone matrix in the calvaria (A), on the bone surface of the tibia and in a very small population within the bone marrow (which we can assume are osteo-progenitor or MSC cells) (B). *Sost/LacZ* was not expressed in hypertrophic chondrocytes in the growth plate (C) nor peripheral regions (D) in the humerus of neonates; *ocy* osteocytes.

Supplementary Fig. 5. Examining Osteoclast Markers. Trabecular regions of 16-week old femurs from the global *Sost* knockout and conditional knockouts were examined by TRAP staining (A). RNAseq of whole femurs from *Sost*^{-/-} showed slightly elevated levels of *Acp5* (TRAP) mRNA (B). Serum levels of RANKL (C) and CTX-1 (D) were also slightly elevated in *Sost*^{-/-} relative to wildtype, but not statistically significant. Serum levels in the conditional mice were not significantly different than the *Cre*-negative controls, for each group.

Table 1. Bone Phenotyping by microCT

Distal Femur Trabecular and Cortical Compartments

Index	<i>Prx1-Cre</i>			<i>Dmp1-Cre</i>			<i>Col1-Cre</i>		
	<i>Cre-</i> (N=6)	<i>Cre+</i> (N=5)	% change	<i>Cre-</i> (N=8)	<i>Cre+</i> (N=6)	% change	<i>Cre-</i> (N=4)	<i>Cre+</i> (N=9)	% change
Trab.TV (mm ³)	3.617±0.543	4.472±0.660*	+23.64	4.460±0.686	5.026±0.445	+12.68	3.957±0.537	4.967±0.755*	+25.52
Trab.BV (mm ³)	0.296±0.190	1.278±0.486*	+333.97	0.700±0.215	1.449±0.532*	+106.89	0.554±0.247	1.252±0.433*	+126.15
Trab.BV/TV (%)	0.078±0.039	0.278±0.081*	+257.86	0.154±0.0307	0.286±0.0987*	+85.83	0.136±0.043	0.247±0.058*	+81.25
Trab.Conn.D. (1/mm ³)	47.42±38.50	96.71±17.30*	+91.30	102.187±23.29	107.37±13.81	+5.07	77.89±30.64	85.31±31.23	+9.53
Trab.SMI	2.897±0.711	1.049±0.735*	-63.77	2.021±0.511	0.858±0.830*	-57.57	2.188±0.811	1.114±0.572*	-49.08
Trab.N (1/mm)	3.470±0.515	4.309±0.371*	+24.18	4.259±0.237	4.590±0.592	+7.77	3.956±0.407	3.859±0.980	-2.45
Trab.Th (mm)	0.049±0.004	0.080±0.011*	+62.92	0.055±0.0039	0.0729±0.009*	+32.52	0.054±0.004	0.070±0.008*	+29.40
Trab.Sp (mm)	0.291±0.049	0.214±0.024*	-26.45	0.228±0.0153	0.198±0.035*	-13.18	0.248±0.029	0.219±0.019*	-11.90
Trab.BMC (µgHA/cm ³)	0.270±0.173	1.221±0.475*	+351.83	0.662±0.210	1.396±0.549*	+111.06	0.531±0.243	1.196±0.434*	+125.02
Cort.TV (mm ²)	7.043±0.770	8.670±1.211*	+23.09	7.722±0.863	8.728±0.567*	+13.03	7.519±0.964	9.176±1.214*	+22.05
Cort.BV (mm ²)	2.782±0.523	3.266±1.464	+17.40	2.777±0.219	3.240±0.308*	+16.69	2.783±0.357	3.498±0.468*	+25.69
Cort.BV/TV (%)	0.393±0.041	0.366±0.137	-6.89	0.362±0.029	0.371±0.026	+2.65	0.370±0.007	0.382±0.020	+3.16
Cort.Th (mm)	0.213±0.0124	0.256±0.036*	+20.18	0.229±0.013	0.236±0.033	+0.03	0.217±0.020	0.265±0.022*	+22.11
Cort.BMC (µgHA/cm ³)	2.909±0.506	3.463±1.529	+19.03	2.990±0.235	3.524±0.356*	+17.86	3.022±0.369	3.800±0.516*	+25.74
Cort.BMD (µgHA/cm ²)	1.048±0.023	1.065±0.022	+1.56	1.077±0.0114	1.087±0.027	+0.96	1.087±0.010	1.086±0.011	-0.03

Cancellous (Trabecular) Bone Compartment of the L4 Vertebrae

Index	<i>Prx1-Cre</i>			<i>Dmp1-Cre</i>			<i>Col1-Cre</i>		
	<i>Cre-</i> (N=6)	<i>Cre+</i> (N=5)	% change	<i>Cre-</i> (N=8)	<i>Cre+</i> (N=6)	% change	<i>Cre-</i> (N=4)	<i>Cre+</i> (N=9)	% change
Trab.TV (mm ³)	1.710±0.048	1.968±0.204*	+15.13	1.889±0.150	1.772±0.249	-6.20	1.978±1.870	1.786±0.193	-9.75
Trab.BV (mm ³)	0.216±0.053	0.395±0.141*	+82.70	0.464±0.077	0.804±0.149*	+73.46	0.396±0.103	0.646±0.128*	+63.22
Trab.BV/TV (%)	0.127±0.030	0.197±0.062*	+55.61	0.241±0.032	0.454±0.0556*	+88.90	0.198±0.037	0.360±0.050*	+81.69
Trab.Conn.D. (1/mm ³)	150.16±45.74	196.39±71.44	+30.79	231.93±29.64	170.98±21.743*	-26.28	217.39±44.74	159.42±23.04*	-26.67
Trab.SMI	1.759±0.287	1.211±0.520*	-31.16	31.62±87.136	-1.225±0.592	-103.87	1.068±0.273	-0.555±0.482*	-151.97
Trab.N (1/mm)	4.233±0.449	4.342±2.007	+2.57	4.591±1.724	6.150±0.389*	+33.95	4.999±0.480	5.402±0.451	+8.071
Trab.Th (mm)	0.040±0.002	0.047±0.006*	+16.36	0.050±0.004	0.074±0.0058	+46.85	0.044±0.004	0.077±0.035	+76.79
Trab.Sp (mm)	0.235±0.028	0.196±0.040	-16.49	0.167±0.053	0.140±0.0127	-16.09	0.192±0.022	0.172±0.017	-10.30
Trab.BMC (µgHA/cm ³)	0.183±0.047	0.344±0.127*	+88.13	0.408±0.077	0.733±0.144*	+79.70	0.342±0.092	0.566±0.117*	+65.42

Data represents mean ± standard deviation for parameters measured. Trab=trabecular; Cort=cortical; BV=Bone Volume; TV=Total Volume; Conn.D.=Connectivity Density; SMI=Structural Model Index; Trab.N=Trabecular Number; Trab.Th=Trabecular Thickness; Trab.Sp=Trabecular Separation; Cort.Th=Cortical Thickness; BMC=Bone Mineral Content; BMD=Bone Mineral Density. *p-values<0.05 compared to own *Cre-* control; data from 16-week old males.

Table 2. *Sost*^{-/-} Bone Phenotyping by microCT

Distal Femur Trabecular and Cortical Compartments

Index	<i>Sost</i> ^{+/+} (N=5)	<i>Sost</i> ^{-/-} (N=7)	% change
Trab.TV (mm ³)	3.884±0.316	4.316±0.234*	+11.12
Trab.BV (mm ³)	0.452±0.092	1.602±0.242*	+254.57
Trab.BV/TV (%)	0.116±0.015	0.371±0.051*	+221.32
Trab.Conn.D. (1/mm ³)	94.736±20.003	113.01±7.24*	+19.30
Trab.SMI	2.557±0.184	0.257±0.386*	-89.94
Trab.N (1/mm)	4.388±0.229	4.755±0.309	+8.35
Trab.Th (mm)	0.048±0.005	0.090±0.007*	+87.23
Trab.Sp (mm)	0.219±0.013	0.178±0.018*	-18.86
Trab.BMC (µgHA/cm ³)	0.422±0.088	1.506±0.238*	+259.44
Cort.TV (mm ³)	6.887±0.327	8.902±0.362*	+29.23
Cort.BV (mm ³)	2.426±0.094	4.123±0.142*	+69.98
Cort.BV/TV (%)	0.352±0.006	0.463±0.010*	+31.53
Cort.Th (mm)	0.197±0.016	0.321±0.012*	+62.94
Cort.BMC (µgHA/cm ³)	2.596±0.073	4.555±0.139*	+75.46
Cort.BMD (µgHA/cm ³)	1.071±0.015	1.105±0.012*	+3.21

Cancellous (Trabecular) Bone Compartment of the L4 Vertebrae

Index	<i>Sost</i> ^{+/+} (N=5)	<i>Sost</i> ^{-/-} (N=7)	% change
Trab.TV (mm ³)	1.694±0.191	1.557±0.193	-8.11
Trab.BV (mm ³)	0.372±0.039	0.934±0.150*	+151.07
Trab.BV/TV (%)	0.220±0.003	0.599±0.042*	+172.49
Trab.Conn.D. (1/mm ³)	243.20±8.512	217.493±35.09	-10.57
Trab.SMI	0.974±0.093	-2.468±0.633*	-353.43
Trab.N (1/mm)	5.383±0.083	7.747±0.314*	+43.93
Trab.Th (mm)	0.044±0.001	0.090±0.008*	+104.73
Trab.Sp (mm)	0.175±0.003	0.104±0.009*	-40.72
Trab.BMC (µgHA/cm ³)	0.330±0.035	0.844±0.142*	+155.46

Data represents mean ± standard deviation for parameters measured. Trab=trabecular; Cort=cortical; Cort.Th= cortical thickness; BV=Bone Volume; TV=Total Volume; Conn.D.=Connectivity Density; SMI=Structural Model Index; Trab.N=Trabecular Number; Trab.Th=Trabecular Thickness; Trab.Sp= Trabecular Separation; BMC=Bone Mineral Content; BMD=Bone Mineral Density. *p-values<0.05; data from 16-week old males.

Table 2. *Sost*^{-/-} Bone Phenotyping by microCT

Distal Femur Trabecular and Cortical Compartments

Index	<i>Sost</i> ^{+/+} (N=5)	<i>Sost</i> ^{-/-} (N=7)	% change
Trab.TV (mm ³)	3.884±0.316	4.316±0.234*	+11.12
Trab.BV (mm ³)	0.452±0.092	1.602±0.242*	+254.57
Trab.BV/TV (%)	0.116±0.015	0.371±0.051*	+221.32
Trab.Conn.D. (1/mm ³)	94.736±20.003	113.01±7.24*	+19.30
Trab.SMI	2.557±0.184	0.257±0.386*	-89.94
Trab.N (1/mm)	4.388±0.229	4.755±0.309	+8.35
Trab.Th (mm)	0.046±0.005	0.090±0.007*	+87.23
Trab.Sp (mm)	0.219±0.013	0.178±0.018*	-18.86
Trab.BMC (µgHA/cm ³)	0.422±0.088	1.506±0.238*	+259.44
Cort.TV (mm ²)	6.887±0.327	8.902±0.362*	+29.23
Cort.BV (mm ²)	2.426±0.094	4.123±0.142*	+69.98
Cort.BV/TV (%)	0.352±0.006	0.463±0.010*	+31.53
Cort.Th (mm)	0.197±0.016	0.321±0.012*	+62.94
Cort.BMC (µgHA/cm ³)	2.596±0.073	4.555±0.139*	+75.46
Cort.BMD (µgHA/cm ³)	1.071±0.015	1.105±0.012*	+3.21

Cancellous (Trabecular) Bone Compartment of the L4 Vertebrae

Index	<i>Sost</i> ^{+/+} (N=5)	<i>Sost</i> ^{-/-} (N=7)	% change
Trab.TV (mm ³)	1.694±0.191	1.557±0.193	-8.11
Trab.BV (mm ³)	0.372±0.039	0.934±0.150*	+151.07
Trab.BV/TV (%)	0.220±0.003	0.599±0.042*	+172.49
Trab.Conn.D. (1/mm ³)	243.20±8.512	217.493±35.09	-10.57
Trab.SMI	0.974±0.093	-2.468±0.633*	-353.43
Trab.N (1/mm)	5.383±0.083	7.747±0.314*	+43.93
Trab.Th (mm)	0.044±0.001	0.090±0.008*	+104.73
Trab.Sp (mm)	0.175±0.003	0.104±0.009*	-40.72
Trab.BMC (µgHA/cm ³)	0.330±0.035	0.844±0.142*	+155.46

Data represents mean ± standard deviation for parameters measured. Trab=trabecular; Cort=cortical; Cort.Th= cortical thickness; BV=Bone Volume; TV=Total Volume; Conn.D.=Connectivity Density; SMI=Structural Model Index; Trab.N=Trabecular Number; Trab.Th=Trabecular Thickness; Trab.Sp= Trabecular Separation; BMC=Bone Mineral Content; BMD=Bone Mineral Density. *p-values≤0.05; data from 16-week old males.

Figure 1

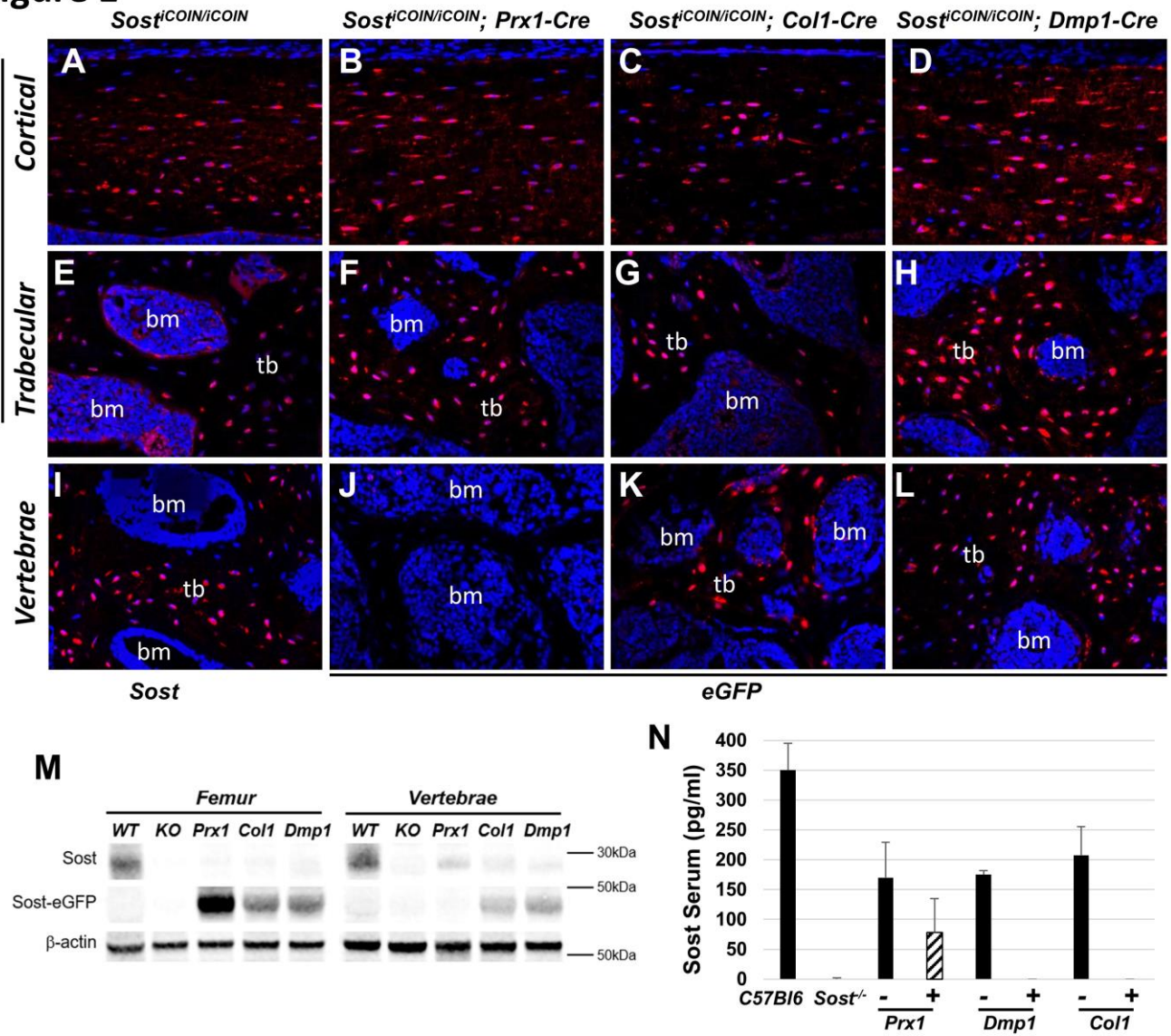


Figure 2

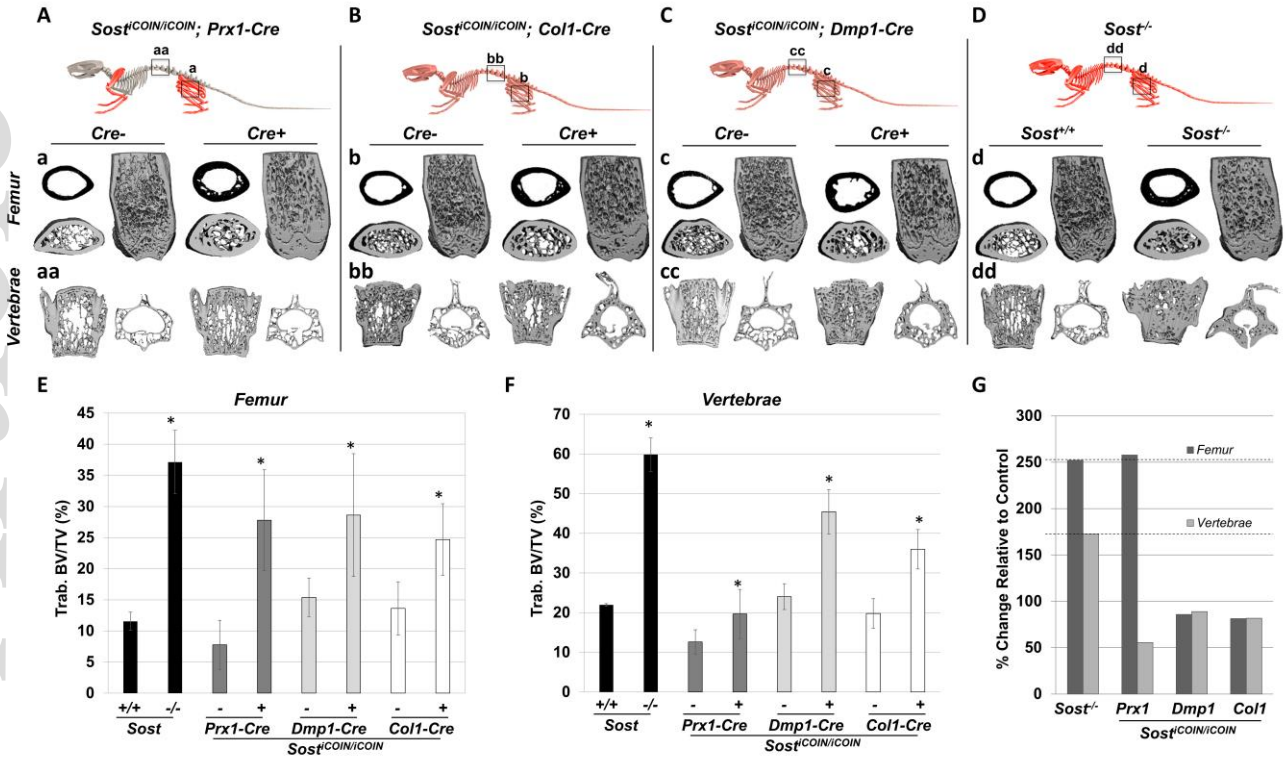


Figure 3

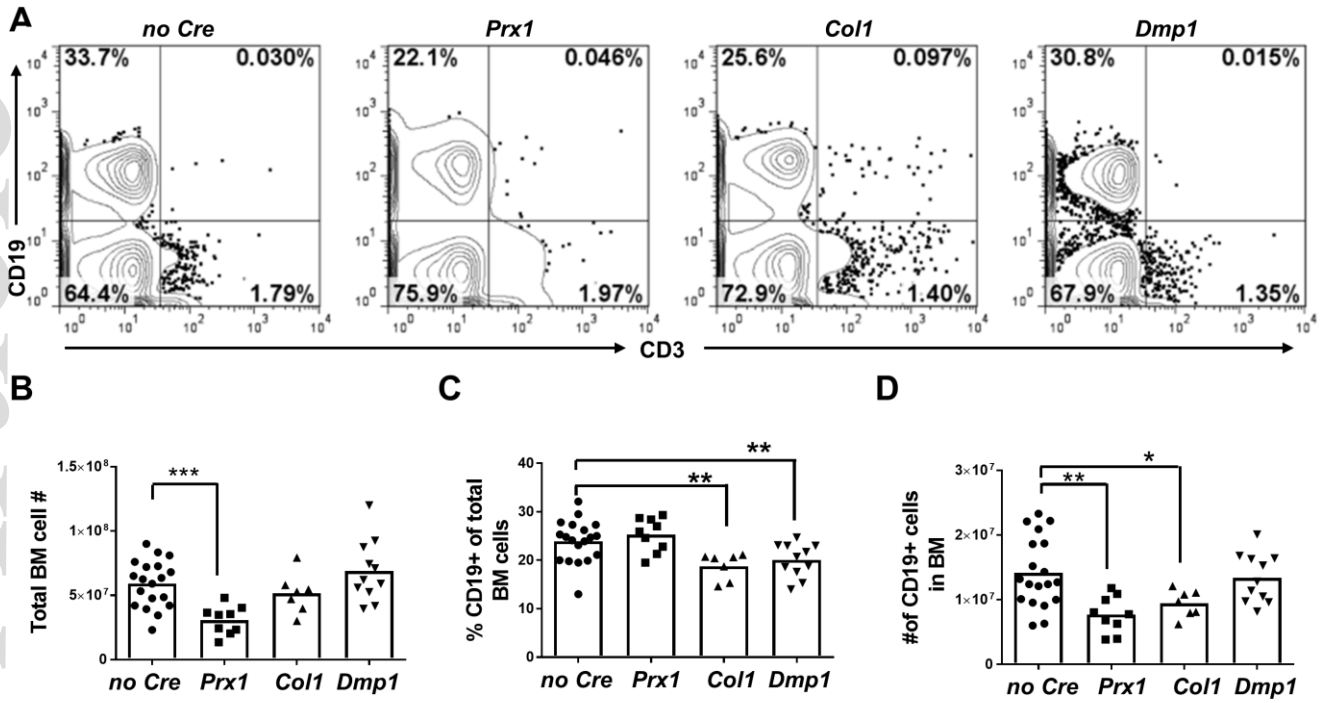


Figure 4

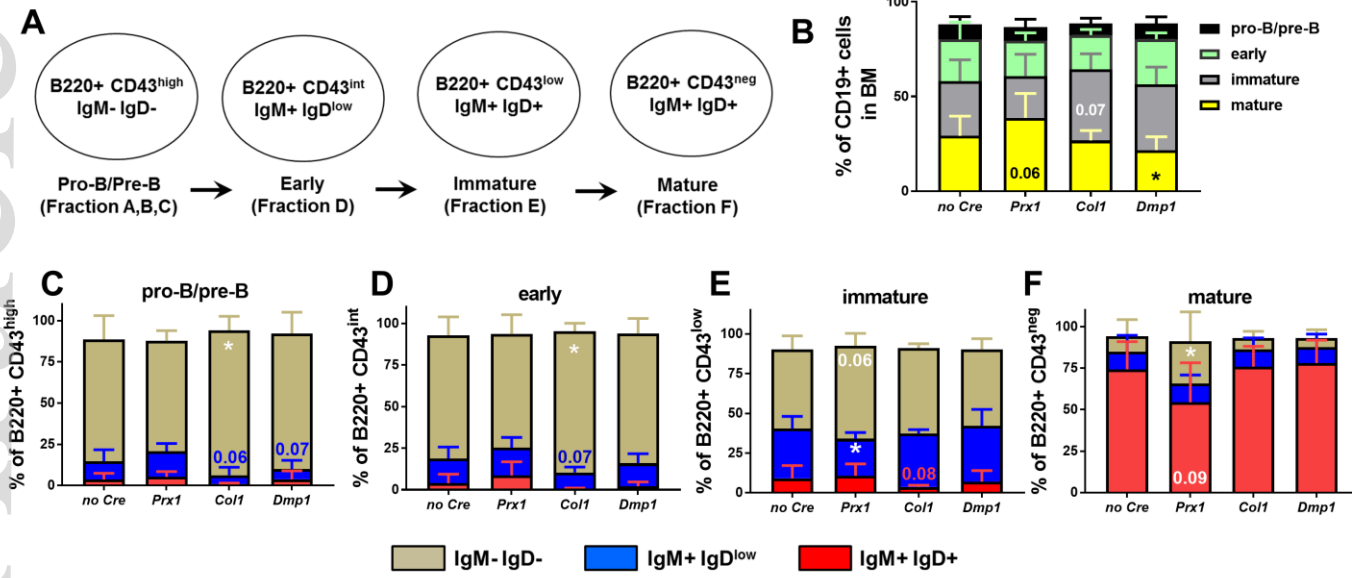


Figure 5

